Development of Global Calibration for Accurate GaAs-PHEMT Simulation

Helmut Brech, *Member, IEEE*, Thomas Grave, and Siegfried Selberherr, *Fellow, IEEE*

***Abstract*—Today's GaAs PHEMTs make it possible to cover applications of an extremely wide frequency range, as high as 100 GHz, with a single device type. In this paper, a set of models and calibrations for the predictive device simulation of GaAs PHEMTs is developed. The simulation setup includes a description of the device geometry. In particular, a realistic representation of the region between the ohmic contacts and the channel is included along with the fitting procedure of the simulation parameters and the necessary transport and interface models. In addition, special emphasis has been placed on a simultaneous fitting of currents and capacitances. The resulting setup allows to describe different devices without changing any nontechnology dependent parameters and thus provides a global calibration within a given device family. This capability is demonstrated by comparing the measured and simulated results of five very different devices which cover gate lengths from 120 to 500 nm, transconductances from 400 to 800 mS/mm, and ungated channel lengths from 70 to 600 nm**

***Index Terms*—Calibration, GaAs, millimeter wave devices, MODFET, semiconductor heterojunctions, simulation.**

I. Introduction

THE GaAs wafer industry has experienced phenomenal growth over the last few years [1]. Today, MESFETs are the working horse for most large volume applications. As the demands on device performance are increased other transistors like pseudomorphic HEMTs (PHEMTs) and HBTs are becoming very important.

PHEMTs on GaAs are able to cover an extremely wide frequency range with very good competitiveness over other technologies. Depending on the application, different requirements arise. The lower important frequency range 0.9/1.9 GHz is used for mobile communication where HEMTs are competing with various other technologies such as LDMOS, Si/Ge-HBTs, III–V-HBTs, and GaAs-MESFETs. Therefore, cheap volume production is one of the most important requirements. These HEMTs will typically have gate lengths between 500 nm and 1 μm and breakdown voltages over 10 V. Frequency bands around 40 GHz for base stations lead to a trade off between RF performance and power capability. HEMTs for applications around 77 GHz and 94 GHz are usually optimized in first place with respect to their RF performance. Therefore, they typically exhibit gate lengths below 150 nm and breakdown voltages around 5 V.

Manuscript received June 20, 2000. The review of this paper was arranged by Editor R. W. Dutton.

H. Brech was with Siemens Corporate Research, D-81739. He is now with Motorola Inc., Semiconductor Product Sector, Tempe, AZ 85284 USA (e-mail: Helmut.Brech@motorola.com).

T. Grave is with Infineon Technologies, D-81606 Munich, Germany.

S. Selberherr is with the Institute for Microelectronics, Technical University Vienna, A-1040, Vienna, Austria.

Publisher Item Identifier S 0018-9383(00)07790-X.

In a production line, it is favorable to cover as many applications as possible with a minimum of process and device variations. In order to react fast on market needs, it is crucial to minimize cycle times and the number of technology runs necessary for the development of a new product. Accurate device simulation can play an important role to meet these requirements. To obtain sufficient predictive capability of simulation, calibration has to be global within a certain technology platform which means that simulation results have to fit well to measurements by adjusting only parameters underlying process uncertainties within realistic ranges. In the following, a combination of simulation models and parameters are established which meet these rigorous requirements.

The first step is to establish a realistic device geometry which will be described in Section III. The different regions of the geometry can be simulated by various models. In Section IV, the appropriate transport models for each semiconductor layer of the device will be investigated. In Section V the verification of the simulation results is described. To obtain a consistent set of parameters for the simulation the results are compared to various data which are measured currents and capacitances extracted from measured S-parameters. The comparison between measured and simulated drain current I_D is performed on the transfer characteristics with $V_{DS} = 2.0\,\mathrm{V}$ because it reveals the most important information on the dc characteristics in only one curve.

To minimize uncertainties the simulation setup is developed for a reference device $\mathrm{HEMT_{ref}}$ which dimensions are known very well from process technology. This device will be used multiple times in the following for investigations and comparisons to other HEMTs. To demonstrate the capabilities of the obtained simulation setup, in Section VI four quite different devices in addition to $\mathrm{HEMT_{ref}}$ will be simulated without changing the simulation setup and the set of parameters. Only quantities with uncertainties given by process technology will be used to fit the simulation results to the measurements.

II. Simulation Models

For all simulations, the simulator MINIMOS-NT was used. The models were described in [2]. For the work presented here only two models should be pointed out, since they are modified and of particular relevance.

For the hydrodynamic transport model the electron mobility is modeled as a function of the carrier temperature T_n, as follows:

$$\mu_n(T_n) = \frac{\mu_n^0}{\left(1 + \alpha_n \cdot \left(\dfrac{T_n - T_L}{T_0}\right)^{(1/\beta)}\right)^{\beta}}. \qquad (1)$$

The temperatures are scaled by some arbitrary temperature T_0. T_L is the lattice temperature. Initially, (1) was developed by Hänsch for silicon [3] where $\beta = 1$. The principal T_{np}^{-1} dependence does not hold for III–V semiconductors. Monte Carlo simulations reveal a dependence between $\mu \propto T_{np}^{-2}$ and $\mu \propto T_{np}^{-5}$ [4], [5], [15], [16]. The parameter β is used in the simulation to model the decay of mobility for moderate carrier temperatures. For $T_n = 0$ and $T_n \to \infty$ the mobility is independent of β.

The second detail to be pointed out is the thermionic field emission model, which reads

$$J_{n2} = q \cdot v_{n2}(T_{n2}) \cdot n_2 - q \cdot \frac{m_{n2}}{m_{n1}} \cdot v_{n1}(T_{n1}) \cdot n_1 \cdot \exp\left(-\frac{\Delta E_C}{k_B \cdot T_{n1}}\right) \cdot f(\delta E_C). \quad (2)$$

The tunneling current through a potential barrier in first order is $j \propto \exp(-(E/k_B T_n))$. Thus, the exponential function in (2) would read $\exp(-(\Delta E_C - \delta E_C/k_B \cdot T_{n1}))$. To describe deviations from the idealized tunneling model the exponential function is expanded into a Taylor series. Therefore $f(\delta E_C)$ in (2) becomes

$$f(\delta E_C) = 1 + \frac{B_1}{1} \cdot \left(\frac{\delta E_C}{k_B T_n}\right) + \frac{B_2}{2} \cdot \left(\frac{\delta E_C}{k_B T_n}\right)^2 + \cdots + \frac{B_i}{i!} \cdot \left(\frac{\delta E_C}{k_B T_n}\right)^i \quad (3)$$

where B_i have to be considered as fitting parameters for the simulation.

A physical reason for the inadequacy of the idealized tunnel characteristics is that the electrons in the whole simulation area are treated as classical particles, i.e., with zero spatial extension. This means that a simulated electron in the channel close to the interface experiences only the properties of the channel material. It is well known from quantum mechanics that the electron wave extends several nanometers which leads to nonlocal effects such as quantization in a potential well [6].

Additionally, in the simulation the electric field is linearly interpolated between grid points. Nonlocal effects described by a local model as well as interpolation errors would lead to a significant overestimation of tunneling without modification of (2).

III. Composition of the Simulated Device Geometry

The composition of the simulation area as well as assumptions for the contacts are very critical for the predictive capabilities of the simulation. In Fig. 1 a typical scanning electron microscope (SEM) photograph of a HEMT is shown. The epitaxial layers cap, supply, channel, and buffer are indicated in the picture. The physical interfaces between the epitaxial layers are considered to be abrupt. The ohmic contacts, source and drain, can be identified by a rough metal/semiconductor interface which is caused by an alloying process. In contrast, the gate Schottky contact exhibits a smooth interface. A schematic representation of the conduction band in a cross section under the gate is shown in Fig. 2.

Note in Fig. 1 that at the ohmic contacts no metal penetrating through the cap layer into the supply or even into the channel layer can be observed. It is discussed that some material which

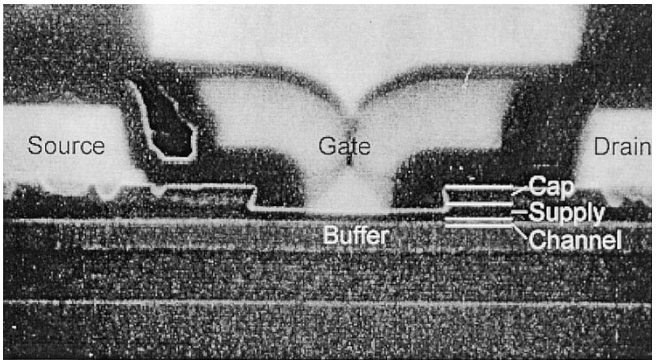

Fig. 1. SEM photograph of a HEMT. The ohmic source and drain contacts can be identified by the alloy penetrating into the cap layers whereas the Schottky gate contact builds a sharp interface.

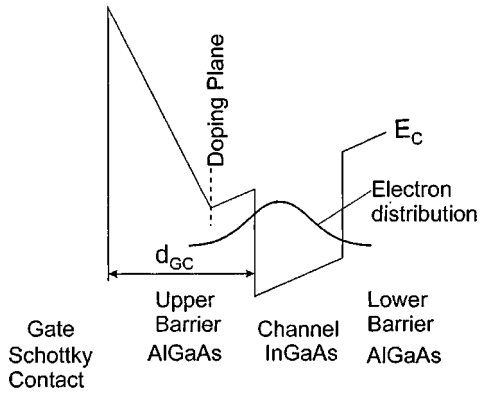

Fig. 2. Schematic conduction band diagram and electron distribution in the channel of a delta doped DH-PHEMT.

behaves like a dopant in the semiconductor might diffuse into the layers or even that metal might reach the channel by spiking. Based on the different assumptions, three simulation models for the ohmic contacts can be developed.

A) Ohmic contact only on top of the cap layers.
B) Ohmic contact on top of the cap layers with high doping between the contacts and the channel.
C) Ohmic contact directly on the channel.

In Fig. 3 a schematic cross section of the investigated $\mathrm{HEMT_{ref}}$ is shown. The hatched areas under the ohmic contacts indicate the regions for which the different models can be used, i.e., nominal specified MBE-grown layers, nominal layers but with doping and contact metal.

In Fig. 4 measured transfer characteristics of $\mathrm{HEMT_{ref}}$ are shown (bold line without symbols) along with three different simulations. All three simulations are performed with the nominal layer sequence, hydrodynamic (HD) transport model in the channel and in the supply, and drift diffusion (DD) transport model in all other semiconductor layers. Electrons can surmount the energy barrier by real space transfer (RST) which is included in all three simulations by applying the HD model in the channel.

Using the contact model (A), i.e., ohmic contacts only on top of the cap layers and a thermionic emission (TE) model which does not include tunneling the simulated current is very low (squared symbols in Fig. 4). Even when a constant doping concentration of $N_D = 3.0 * 10^{18}\ \mathrm{cm}^{-3}$ is added in the simulation

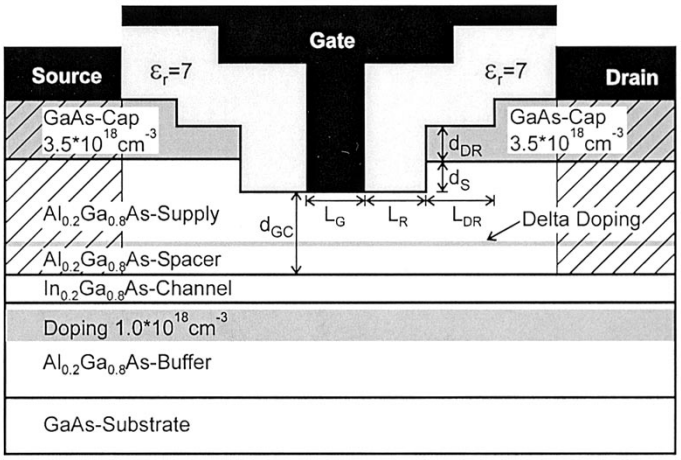

Fig. 3. Schematic cross section of the simulated HEMTref. The region for which different models are investigated are indicated by the hatched areas.

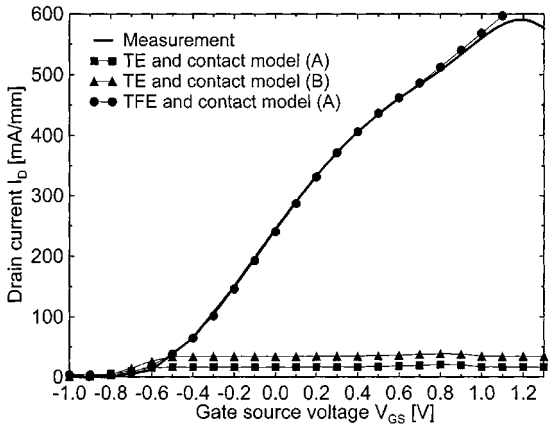

Fig. 4. Measured and simulated transfer characteristics. The simulations are performed with the nominal layer structure and an interface model with and without tunneling.

[contact model (B)] the characteristics are not improved significantly (triangle symbols in Fig. 4). For the simulation applying a thermionic field emission (TFE) interface model without additional doping the simulated and measured data (circles and bold line in Fig. 4) agree very well such that the two curves are on top of each other for the most part of the characteristics.

As described before the third possible approach for the ohmic contacts of HEMTs is based on the assumption that metal from the ohmic contacts spikes through the AlGaAs supply layer facilitating an ohmic contact directly on the channel [contact model (C)]. In this case, most electrons would not have to cross the energy barrier between the channel and the supply but would be conducted directly from source through the channel to the drain. This is a quite commonly used assumption for heterostructure devices [7]–[9].

Two aspects of this model will be investigated in the following. The first is the consequences of this contact model on the simulated current transport in HEMTs and the resulting characteristics. The second aspect is experimental results to gain more insight into the ohmic contacts of manufactured HEMTs.

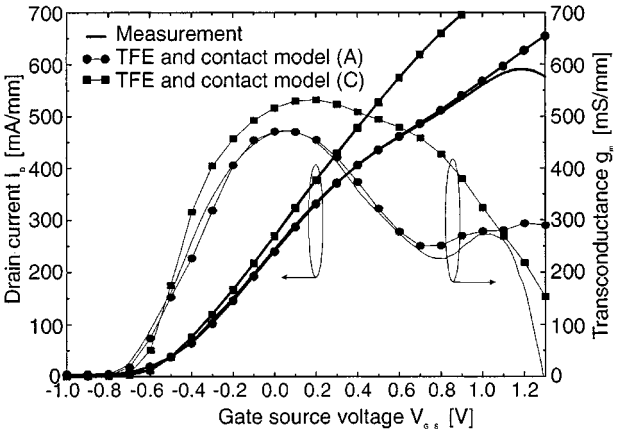

Fig. 5. Measured and simulated drain current and transconductance. The simulations are performed with different geometric contact models. With source and drain contacts directly on the channel and source and drain only on top of the cap layers.

In Fig. 5, simulation results of the device with ohmic contacts directly on the channel [contact model (C)] are compared with simulation results of the device with nominal layer structure [contact model (A)]. Both simulations were performed using the TFE interface model. The threshold voltage of the simulation with directly contacted channel was adjusted by assuming a 10% lower delta doping concentration than for the simulation with contacts only on the cap. The experimental results of $\mathrm{HEMT_{ref}}$ and the two simulated characteristics are very similar near V_T. But for $V_{GS} > 0.0$ V the current in case of model (C) is much higher than in case of model (A) as well as the measured values.

The magnitude of the maximum transconductance $g_{m\,\max}$ and the V_{GS} where it is reached is among the most important dc parameters. Both are overestimated if the channel is contacted directly as shown in Fig. 5. Moreover, neither the reduction in g_m for $V_{GS} > 0.0$ V nor the second local maximum in g_m, which refers to the parasitic MESFET, is reproduced. Using contact model (A) the simulated and measured characteristics compare very well.

The different setups for the ohmic contacts lead to significant differences in the simulated carrier transport properties of the HEMTs. In Figs. 6 and 8 the current distributions for the two cases are shown both for $V_{DS} = 2.0$ V and $V_{GS} = 0.5$ V. This corresponds to a bias point between the two local maxima of the transconductance given in Fig. 5. In both cases the channel can be identified by the layer with the highest current density.

If the ohmic contacts are directly on the channel as shown in Fig. 6 most of the electrons flow directly from source through the channel to the drain contact. Therefore the current through the channel is still governed almost linearly by the gate and (RST) is underestimated. If the contact resistance in the simulation would be reduced to zero and the current flow over heterojunctions prevented (no tunneling) this would correspond to the intrinsic transistor.

If the contacts are only on top of the cap layers as shown in Fig. 8 the electrons have to cross the energy barrier between the channel and the supply beneath the end of the gate. Moreover, for high currents the electrons heat up and start to surmount

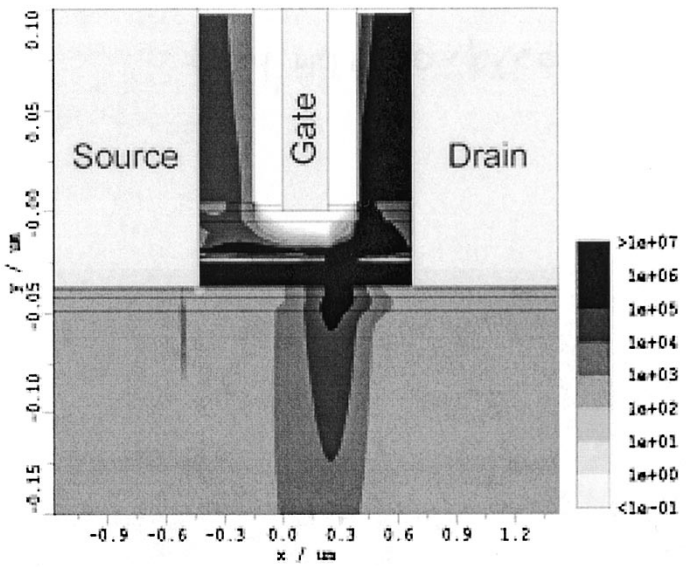

Fig. 6. Current density of the HEMT geometry with directly contacted channel at $VDS = 2.0$ V and $VGS = 0.5$ V. In addition to the current conducted through the cap a large fraction is conducted directly from source through the channel to the drain. The geometry is not in linear scale.

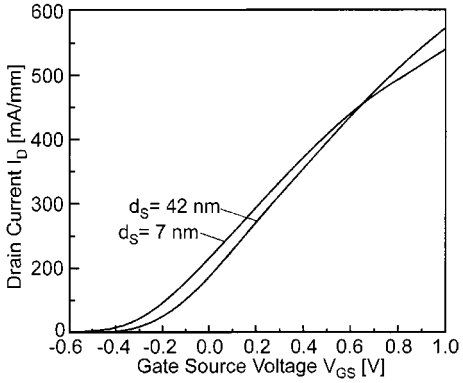

Fig. 7. Measured transfer characteristics of two devices which differ only in their thickness of undoped AlGaAs supply layer between the ohmic contacts and the channel.

the barrier already under the gate. Therefore more current is conducted in the barrier layers where their mobility is rather low and thus g_m is reduced. This effect is not only important for modeling the transfer characteristics but essential to describe short channel effects.

More evidence that the contact model (A) is a very realistic assumption is obtained by aspects obtained from experimental results. The directly contacted channel model [contact model (C)] relies on the assumption that contact metal spikes through the cap and the barrier layers along with doping high enough to facilitate an ohmic contact to the channel. This mechanism either depends on the thickness of the cap and the barrier layers through which spiking should occur, or the spiking has to be much deeper than the thickness variations of the layers between ohmic contact and channel.

To investigate this issue, two PHEMTs with double recess were fabricated which basically differ only in the thickness d_S of 7 nm and 42 nm indicated in Fig. 3. In Fig. 7 the measured transfer characteristics of the two devices are shown. The two

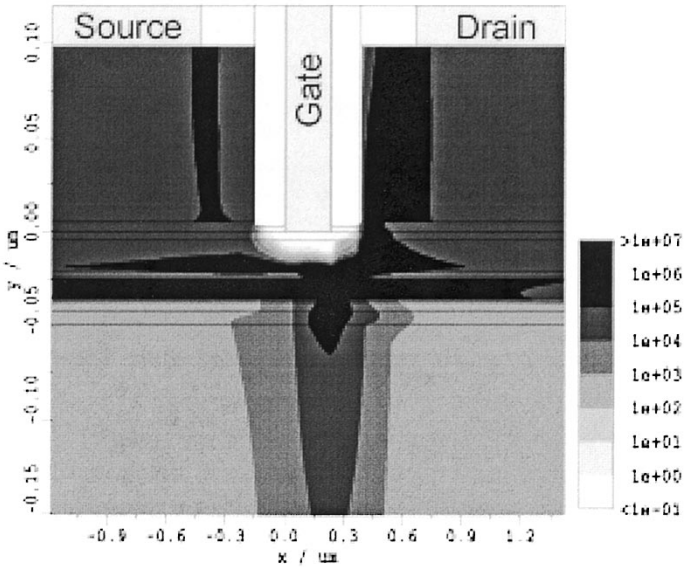

Fig. 8. Current density of the HEMT geometry with contacts only on top of the cap layer at $VDS = 2.0$ V and $VGS = 0.5$ V. All electrons from the channel which contribute to ID have to be partially conducted in AlGaAs layers. The geometry is not in linear scale.

PHEMTs were produced in different technology runs which resulted in a shift of V_T due to slightly different recess depths. A more positive V_T, obtained for the device with $d_S = 42$ nm, usually leads to a higher $g_{m\,\max}$ but to a lower $I_{D\,\max}$. In addition to a more positive V_T this device has a 35 nm larger d_S than the other device, but $I_{D\,\max}$ is significantly larger. If the depth of spiking would be in the order of 120 nm (thickness of cap and supply) one would expect a reduced $I_{D\,\max}$. Thus, if spiking is an appropriate assumption the depth has to be much deeper than 120 nm. It is believed that the reason for the enhanced $I_{D\,\max}$ is a reduction in crystal damage which usually occurs by etching the double recess in the cap layer.

To close the chain of proof against spiking the depth of the ohmic contact metal penetrating into the semiconductor is estimated. Fig. 9 shows a SEM photograph of a HEMT with alloyed ohmic contacts from the bottom. With a special preparation technique the semiconductor was removed. The T-shaped gate finger can be clearly identified between the ohmic source and drain metals. The light spots on the ohmic contacts show some remaining semiconductor material. The dimensions can be estimated by comparison to the gate length which is about 200 nm. It is evident that the total contact area is much smoother than 200 nm. Therefore, it is clear that the HEMT cross section shown on the SEM photograph in Fig. 1 is not a coincidental but a very typical one.

Nonalloyed ohmic contacts on top of the cap layer have led to very good HEMT characteristics for InP based HEMTs [10], [11]. This is another argument that contacting the channel is not a prerequisite for excellent performance. In our case, sufficient evidence has be given for the contact model (A). It was proven that the simulation of the nominal given layer sequence with a thermionic field emission interface model is well suited to describe the dc characteristics of the different HEMT's discussed here. Therefore this setup will be used for all following simulations.

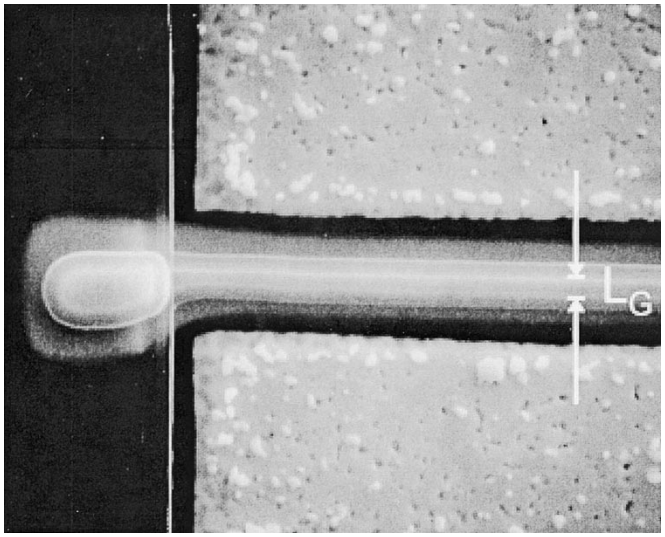

Fig. 9. SEM picture of the contact metals of a HEMT from the backside with removed semiconductor. A gate finger as well as alloyed ohmic contacts on both sides are shown. Some remaining GaAs can be observed by the lighter spots on source and drain.

IV. Determination of the Transport Models

In the following section, different combinations of transport models will be investigated. Some models can lead to significant increase in computation time or to convergence problems. Therefore, it is necessary to find the optimum combination of models.

In HEMTs, current transport in three main layers under the gate has to be considered, namely in the barrier layer below the channel, in the channel itself, and in the upper barrier layer. The impact of employing different transport models in these layers will be shown for $\mathrm{HEMT_{ref}}$.

In Fig. 10, measurements and simulations of the transfer characteristics are compared. One simulation is performed with a DD transport model in all semiconductor layers. This is compared to simulations were either in the channel or in both the channel and the supply layer a HD model is used. In any case, the DD model is used for all other semiconductor layers.

The measured and all three simulated transfer characteristics exhibit the same V_{th}. The simulation with the DD model in all semiconductor layers shows the lowest I_D and an almost constant g_m. This is due to the fact that no velocity overshoot is taken into account. Therefore, the average electron velocity is lower than in the cases were a HD model is employed. Using the HD model only in the channel and the DD model in all other semiconductor layers (squares in Figs. 10 and 11) the current increases more rapidly up to a V_{GS} of about 0.5 V. This part of the I_D and g_m characteristics coincides very well with the measured data. For $V_{GS} > 0.5$ V, however, I_D and g_m are too low, similar to the case of pure DD transport. Again the same problem arises that no velocity overshoot is taken into account in the supply layers.

If the HD model is applied in the channel and the supply layer (triangles in Figs. 10 and 11) the simulated I_D and g_m coincide extremely well with measurements. In this case even the second maximum in g_m appears which is related to the parasitic MESFET. However, due to an underestimation of the gate

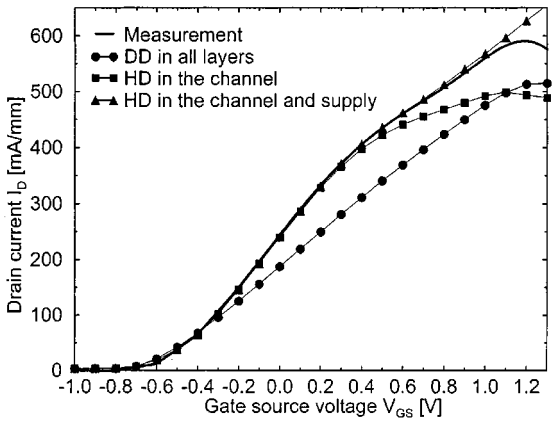

Fig. 10. Measured and simulated transfer characteristics for different transport models. Circles indicate DD in all layers, squares HD in the channel and DD in the remaining layers, and triangles HD in the channel and supply layer, DD in the remaining layers.

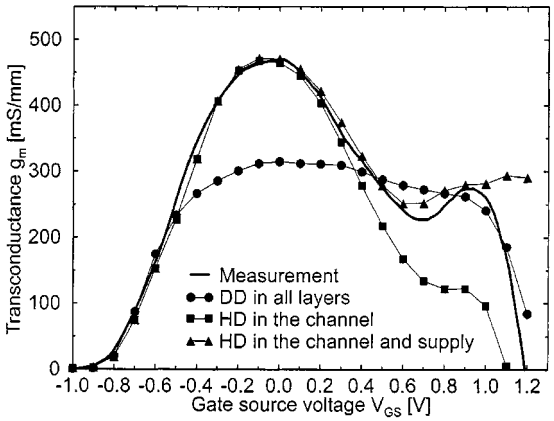

Fig. 11. Measured and simulated transconductance for different transport models. Circles indicate DD in all layers, squares HD in the channel and DD in the remaining layers, and triangles HD in the channel and supply layer, DD in the remaining layers.

current, the additional reduction is not reproduced very well. Also thermal effects become significant which are not included in the simulation. This issue will be further addressed in Section V. It appears that the simulation setup with the HD model in the channel and the supply layer is able to reproduce almost the entire V_{GS} range.

Based on these results, it seems that the HD model would also be favorable for the buffer layer. The simulations shown in Figs. 10 and 11 reveal slightly higher simulated than measured current values even with only a DD model applied in the lower barrier layer. To achieve agreement between simulation and measurements, an unrealistically low saturation velocity has to be used in the DD model for the buffer. The simulation of the subthreshold region is a common problem in device simulation. As a physical reason it is discussed that the carriers might be better confined in the channel due to quantization effects than assumed in the bulk model [12]. Therefore, the DD model will be used in the buffer layer for all further simulations.

The results discussed so far show that the simulation setup presented in Sections III and IV (i. e. contacts on top of the cap layer, a TFE interface model, and the HD model in the channel

and the supply layer) is able to model the most important device characteristics very well.

V. Fitting Procedure

In the following, section the geometrical setup and the transport models described above will be used. The structure of a real device after the process is known only with a certain accuracy. Therefore, the simulation results have to be fitted to the measurements by adjusting these parameters.

The basic problem of the fitting procedure is, that the set of unknowns is large enough that a given characteristics can be modeled by different combinations of geometry and model parameters. For instance a certain current density j can be obtained by different products of carrier concentrations and velocities $n \cdot v$. Therefore, not only the drain current but simultaneously the gate capacitances was calibrated versus V_{GS}. This way a certain distinction between carrier concentration and velocity can be made which reduces uncertainties substantially and, thus, increases the predictive capabilities.

A. Simulation of the Transfer Characteristics

The fitting procedure uses only parameters which are subject to process uncertainties within realistic ranges such as the effective barrier height of the gate Schottky contact Φ_B, the location and concentration of the doping in the supply N_{DS} and in the buffer layer N_{DB} as well as the gate to channel separation d_{GC} to fit the threshold voltage V_T. Fitting the transfer characteristics for $V_{GS} > V_T$ both the carrier concentrations and the velocities have to be simulated. The electron velocity in MINIMOS-NT is determined by the mobility and the driving force [2]. In the HD model the reduction of the mobility in the high field regime is modeled by the electron temperature as shown in (1). Therefore, τ_ω, v_n^{sat}, and β are fitting parameters for the electron velocity.

The simulation of the parasitic MESFET region is basically related to the transport model used in the supply layer as described in Section IV. As shown a HD model in the AlGaAs supply layer is necessary to model the second local maximum in g_m. The quantities v_{sat}, β, and τ_ω for AlGaAs are used as the fitting parameters.

Electron concentration and velocity can be separated by considering both the $I_D(V_{GS})$ and the $C_G(V_{GS})$ characteristics. An increase in carrier concentrations leads to an increase in both I_D and C_G, but an increase in carrier velocity leads to an increase in I_D and to a decrease in C_G. Therefore, a simultaneous fit of both gate capacitance and current characteristics has to be considered.

In Fig. 12 the gate capacitance extracted from S-parameter measurements of HEMT_{ref} is shown along with simulated C_G curves. Also, the corresponding measured and simulated values of g_m are depicted which correspond to the measured data in Fig. 11.

As a previous result, DD transport in the supply layer revealed too low I_D for $V_{GS} > 0.2$ V. This is due to the relatively low velocity of electrons in the supply layer for this model. Whereas for $V_{GS} < 0.2$ V no difference in I_D could be observed and only a minor difference occurred in g_m, the C_G applying DD transport in the supply layer differs significantly from the C_G obtained with a HD model in the supply as depicted in Fig. 12. This shows that the capacitances are extremely sensitive to carrier density and velocity.

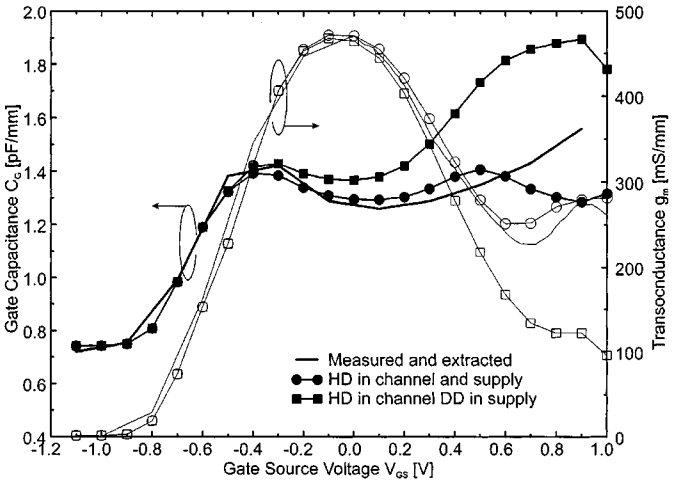

Fig. 12. Gate capacitance extracted from S-parameter measurements and mixed DD/HD simulations using a quasistatic approximation at $VDS = 2.0$ V. An increase in electron velocity reduces CG but increases ID. This way the electron velocity can be separated from the electron concentration.

If a HD model is applied in the supply layer both the g_m and C_G characteristics improve. For $V_{GS} < 0.6$ V both characteristics are within $\pm 5\%$ of the measured and extracted data, respectively. This was obtained by fitting τ_ω, v_n^{sat}, and β for both the InGaAs and AlGaAs material.

For $V_{GS} > 0.6$ V the measured and simulated current characteristics agree well if a HD model is used in the supply but C_G deviates significantly from the extracted values. The reasons for this insufficient characteristics are manifold and include the following. The interface charge density between semiconductor and passivation is taken to be constant which might not hold for high gate voltages. The HD mobility model must be improved according to [4] were additional effects specific to the mobility of III–V material are proposed. This will have a significant impact on the carrier velocity and density similar to the differences observed for DD and HD and therefore influence C_G. Finally, the impact of the semiconductor heterojunction interface model and thermal effects on the output characteristics which will be illustrated in the following section.

B. Simulation of the Output Characteristics

Fig. 13 shows the simulated output characteristics indicated by circles along with measured data. As depicted, the characteristics agree quite well for $V_{DS} < 2.0$ V and $V_{GS} < 0.6$ V. The discrepancy between simulation and measurements for $V_{DS} < 1.0$ V and $V_{GS} > 0.2$ V is related to the interface model and the transport model in the channel. With the applied models and the corresponding fitting parameters it was not possible to reproduce this part of the output characteristics very well.

For larger V_{DS} g_0 in Fig. 13 is underestimated because impact ionization is not included in the simulation [13]. For high V_{GS} the measured results show a negative gradient which is most likely due to temperature effects as the device heats up and the transport properties are deteriorated. This, in return, reduces the current. Temperature effects are not included in the simulation.

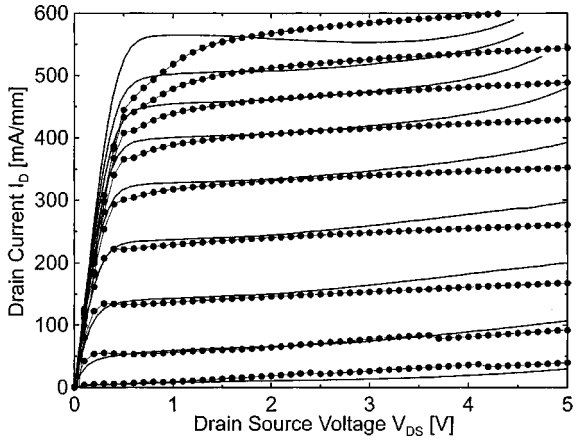

Fig. 13. Measured (lines without symbols) and simulated (lines with circles) output characteristics of $\mathrm{HEMT_{ref}}$. The characteristics with the highest currents are obtained for $VGS = 1.0$ V. The remaining curves are separated by $VGS = 0.2$ V.

TABLE I
PARAMETERS USED FOR SIMULATION OF ALL DH-PHEMTS

Schottky contact barrier height Φ_B	610 meV
Interface charge density	$1.0*10^{12}$cm^{-2}
Relative passivation permittivity	7.0
Low field mobility GaAs	1000 cm^2/Vs
Saturation velocity GaAs	$0.7*10^7$cm/s
Low field mobility AlGaAs	1000 cm^2/Vs
Saturation velocity AlGaAs	$0.7*10^7$cm/s
HD fitting parameter β AlGaAs	0.6
Relaxation time τ_ω AlGaAs	0.1 ps
Low field mobility InGaAs	6000 cm^2/Vs
Saturation velocity InGaAs	$1.1*10^7$cm/s
HD fitting parameter β InGaAs	0.9
Relaxation time τ_ω InGaAs	0.17 ps
Effective tunnel length	7 nm
Coefficients of tunneling Taylor series B_i	$B_{1,2} = 1.0$, $B_{i>2} = 0.0$

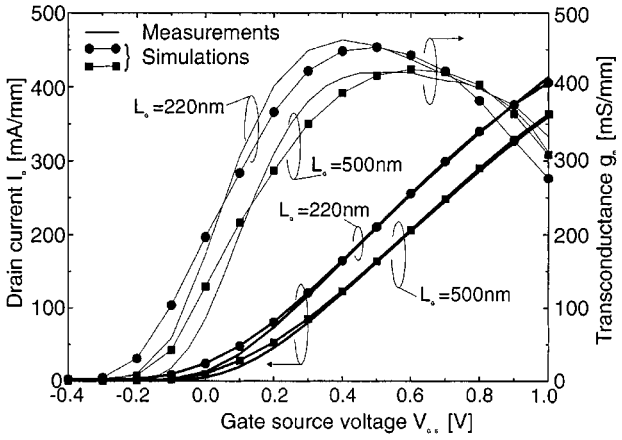

Fig. 14. Simulated (line with symbols) and measured (line without symbols) Drain current ID and transconductance gm at $VDS = 2.0$ V.

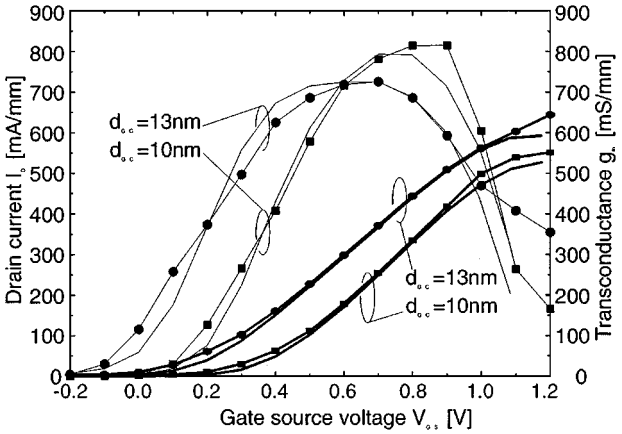

Fig. 15. Simulated (lines without symbols) and measured (lines with symbols) Drain current ID and transconductance gm at $VDS = 2.0$ V of two millimeter wave HEMTs with different recess depths.

They can account for more than 10% change in I_D at $V_{DS} = 5.0$ V [14].

The parameters which provided the best simultaneous fit between simulated and all other investigated characteristics are given in Table I. These parameters and all other in the simulation which do not have technological uncertainties remain unchanged for all other devices. More detailed information on the fitting procedure can be found in [15].

VI. SIMULATION OF POWER AND RF DEVICES

To demonstrate the capabilities of the simulation setup four different devices are simulated and compared to measured dc data. Two power devices are produced on the same wafer which differ only in their gate length and two RF devices which differ only in their gate to channel separation.

In Fig. 14 $I_D(V_{GS})$ and $g_m(V_{GS})$ of the power devices are shown. The simulation of the device with $L_G = 220$ nm was fitted to the measurements only by changing parameters which are technology dependent well within realistic ranges. The results of the second device are obtained by only changing L_G without any additional fitting. As shown both characteristics compare very well with the measured data.

In Fig. 15 the transfer characteristics and the transconductance of two RF devices both with $L_G = 120$ nm are shown. Both devices have been produced on the same wafer. Due to inhomogenities in the recess depth, they exhibit different characteristics. The simulation of the device with $d_{GC} = 13$ nm was again fitted to measured results as described above. The characteristics of the second device are obtained only by changing d_{GC} to 10 nm. Fig. 15 shows that even the device with an extremely small d_{GC} is simulated very well.

More detailed measurement and simulation dc and RF results on both the power and RF devices can be found in [15].

VII. CONCLUSIONS

We have presented a simulation setup that is capable of predictively simulating GaAs-based PHEMTs with high accuracy. For the simulation setup, it is shown that the device geometry used for simulation is extremely important. We have demonstrated that no additional assumptions regarding the contact to the channel should be made other than the nominal given layer sequence, i.e., ohmic contacts only on top of the cap layer. To simulate the transfer characteristic, a hydrodynamic transport model at least in the channel is necessary. To accurately describe

the device behavior for higher V_{GS} also a hydrodynamic model should be used in the supply layer. To find appropriate simulation parameters, we did not only compare simulated and measured currents but also extracted and simulated capacitances. This is extremely important, since this way the carrier concentration can be separated from the velocity. To demonstrate the capabilities of this simulation setup, measurements and simulations of five HEMT's with different epitaxial structures and quite different geometries are presented. All devices were simulated with only one consistent set of simulation parameters. To fit simulation and measurement, only parameters were used which have technological uncertainties all well within realistic ranges.

Thus, simulation is able to meet the rigorous and inevitable requirements for predictive simulation of PHEMTs. This makes it an extremely useful and practical tool not only to optimize device performance but also to reduce technological effort by optimization of performance, yield and cost.

ACKNOWLEDGMENT

The authors would like to thank T. Simlinger, H. Siweris, and A. Werthof for many fruitful discussions as well as A. Stemmer and H. Tischer for dc and RF measurements.

REFERENCES

[1] E. J. Lum, "GaAs technology rides the wireless wave," in *IEEE GaAs IC Symp. Tech. Dig.*, 1997, pp. 11–13.

[2] T. Simlinger, H. Brech, T. Grave, and S. Selberherr, "Simulation of submicron double-heterojunction high electron mobility transistors with MINIMOS-NT," *IEEE Trans. Electron Devices*, vol. 44, pp. 700–707, May 1997.

[3] W. Hänsch and M. Miura-Mattausch, "The hot-electron problem in small semiconductor devices," *J. Appl. Phys.*, vol. 60, pp. 650–656, 1986.

[4] H. Kosina and T. Simlinger, "Modeling concepts for modern semiconductor devices," in *CAS'95—Proc. 1995 Int. Semiconductor Conf.* , Sinaia, Romania, 1995, pp. 27–36.

[5] C. Köpf, H. Kosina, and S. Selberherr, "Mobility model for III–V compounds suited for hydrodynamic device simulation," in *Compound Semiconductors 1995*.

[6] K. J. Ebeling, *Integrierte Optoelektronik*. Berlin, Germany: Springer-Verlag, 1989.

[7] S.-T. Fu, S.-M. J. Liu, and M. B. Das, "Determination of equivalent network parameters of short-gate-length modulation-doped field-effect transistors," *IEEE Trans. Electron Devices*, vol. 37, pp. 888–901, Apr. 1990.

[8] Y.-J. Chan and M.-T. Yang, "$Al_{0.3}Ga_{0.7}As/In_xGa_{1-x}As$ ($0 < x < 0.25$) doped-channel field-effect transistors (DCFET's)," *IEEE Trans. Electron Devices*, vol. 42, pp. 1745–1749, Oct. 1995.

[9] J. Mateos *et al.*, "Influence of real-space transfer on transit time and noise in HEMTs," in *Proc. ESSDERC'—26th Eur. Solid-State Device Research Conf.*, G. Baccarani and M. Rudan, Eds. Gif-sur-Yvette, France: Editions Frontiers, 1996, pp. 745–748.

[10] K. J. Chen *et al.*, "High-performance InP-based enhancement-mode HEMT's using nonalloyed ohmic contacts and Pt-based buried-gate technologies," *IEEE Trans. Electron Devices*, vol. 43, pp. 252–257, Feb. 1996.

[11] K. Higuchi, M. Mori, M. Kudo, and T. Mishima, "New low contact resistance triple capping layer enabling very high G_m InAlAs/InGaAs HEMTs," *J. Electron. Mater.*, vol. 25, no. 4, pp. 643–647, 1996.

[12] C. Moglestue, "A Monte Carlo particle simulation of quantum transport in MODFETs," in *Proc. 9th III–V Semiconductor Device Simulation Workshop*, Heeze, The Netherlands, May 1996.

[13] G. Meneghesso *et al.*, "Study of breakdown mechanism in 2D MESFET's," in *Proc.WOCSDICE*, 1997, pp. 21–22.

[14] Y. Okamoto, K. Matsunaga, M. Kuzuhara, and M. Kanamori, "Novel InGaP/AlGaAs/InGaAs heterojunction FET for X-Ku band power applications," in *1997 IEEE MTT-S Dig.*, pp. 1191–1194.

[15] H. Brech, "Optimization of GaAs based high electron mobility transistors by numerical simulations," Ph.D. dissertation, Tech. Univ. Vienna, Vienna, Austria.

[16] C. Köpf, H. Kosina, and S. Selberherr, "Mobility model for III–V compounds suited for hydrodynamic device simulation," in *Proc. Inst. Physics Conf.*, Cheju Island, Korea, 1995, pp. 1255–1260.

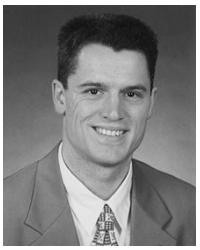

Helmut Brech (M'99) was born in Schwäbisch Gmünd, Germany, in 1968. He received the M.S. degree in electrical engineering from the University of Ulm, Germany, in 1995, and the Ph.D. degree from the Technical University Vienna, Austria, in 1998. His M.S. thesis was devoted to fabrication and characterization of long wavelength lasers on GaAs.

From 1995 to 1998, he worked on GaAs-PHEMT device simulation at Siemens Corporate Research in Munich, Germany. In 1998, he joined the Front-End Technology Simulation Group at Motorola, Austin, TX, working on CMOS and RF-LDMOS process and device simulation. Since March 2000, he has been with Motorola's Wireless Infrastructure Systems Division, Tempe, AZ, engaged in the development of silicon RF power technology.

Thomas Grave was born in Frankfurt, Germany, in 1951. He received the Dipl. degree in physics and the Dr. rer. nat. degree from the University of Heidelberg, Germany, in 1975 and 1979, respectively.

From 1979 to 1983, he was an Assistant Researcher at the Institute of Applied Physics, University of Heidelberg, working on optoelectronic and nonlinear optical effects in Ge and InSb. In 1983 and 1984, he was with the Max Planck Institute for Plasma Physics, Garching, Germany, where he participated in nuclear fusion research. In 1984, he joined the III–V electronics department of Siemens Corporate Technology, where he first was responsible for MESFET process development. This included the technology of a GaAs 1 K SRAM and a SAGFET process applied to analog-to-digital converter ICs. Since 1992, he has been engaged in the development of GaAs-based PHEMTs for low-noise, power, and millimeter wave applications. In November 1997, he changed from Siemens Corporate Technology to the Siemens Semiconductor Group (now Infineon Technologies),Munich, Germany, where he presently continues his work as HEMT Technology Project Manager.

Siegfried Selberherr (M'79–SM'84–F'93) was born in Klosterneuburg, Austria, in 1955. He received the Diplomingenieur degree in electrical engineering and the Ph.D. degree in technical sciences from the Technical University (TU) Vienna in 1978 and 1981, respectively.

He has been holding the *venia docendi* on computer-aided design since 1984 at TU. Since 1988, he has been the Head of the Institut für Mikroelektronik and since 1999 he is dean of the Fakultät für Elektrotechnik. His current topics are modeling and simulation of problems for microelectronics engineering.